Self-Assembly in a Catanionic Mixture with an Aminoacid-Derived Surfactant: From Mixed Micelles to Spontaneous Vesicles

Rodrigo O. Brito,[†] Eduardo F. Marques,*[,†] Paula Gomes,[†] Soraia Falcão,[†] and Olle Söderman[‡]

Centro de Investigação em Química, Department of Chemistry, Faculty of Sciences, University of Porto, Rua do Campo Alegre, No. 687, P-4169-007 Porto, Portugal, and Physical Chemistry 1, Centre for Chemistry and Chemical Engineering, Lund University, P.O. Box 124, SE-22100 Lund, Sweden

Received: March 29, 2006; In Final Form: July 13, 2006

The aqueous self-assembly of a novel lysine-derived surfactant with a gemini-like architecture, designated here as 12-Lys-12, has been experimentally investigated for the amphiphile alone in water and in a mixture with dodecyltrimethylammonium bromide (DTAB). The neat surfactant forms interesting micrometer-sized rigid tubules in the dilute region, resulting in very viscous solutions. For the catanionic mixture with DTAB, various single and multiphase regions were identified (up to a total surfactant concentration of 1.5 wt %) by means of combined polarizing light microscopy, cryo-TEM, and NMR. In the DTAB-rich side, for a mixing molar ratio in the range $2 < \text{DTAB/12-Lys-12} < 4$, a region of stable, unilamellar vesicles can be found. Furthermore, it was found that upon addition of 12-Lys-12 to pure DTAB solutions, the mixed micelles grow and beyond a given mixing ratio, vesicles assemble and coexist with small micelles. The transition is not continuous, since there is a narrow mixing range where phase separation occurs. Self-diffusion measurements and cryo-TEM imaging show that the average vesicle radius is on the order of 30−40 nm.

1. Introduction

Surfactants with enhanced compatibility with living systems are of great potential for pharmaceutical and medical applications. Gemini or dimeric surfactants are highly efficient from a technical viewpoint, due to their low CMCs and enhanced surface activity.[1,2] Amino acid-derived gemini amphiphiles, in particular, seem to have the additional potential of being biologically and environmentally amiable.[3−5] In this work, a new anionic pseudogemini surfactant, derived from the amino acid lysine, was synthesized. The compound sodium N^{α},N^{ϵ}-didodecanoyl-L-lysinate (12-Lys-12) has two saturated C_{12} alkyl chains and the side chain of the amino acid effectively acts as a covalent spacer (Figure 1). This molecular architecture thus closely resembles that of a heterogemini compound. For this type of amino acid-derived amphiphile, besides electrostatic and hydrophobic interactions determining the aqueous self-assembly, hydrogen bonding between headgroups also plays a crucial role, opening up the possibility of formation of colloidal aggregates with relatively uncommon features, such as fibers and tubules.[6−9] Such structures are not only of fundamental interest but may have important technical applications, inter alia as scaffolds for supported catalysis, molecular nanotemplates, and gelators.

Catanionic vesicles, i.e., vesicles formed by mixed cationic and anionic amphiphiles, have been extensively investigated in the last fifteen years due to their interest from a fundamental point of view[10−20] and great potential in several applications, such as drug and gene delivery,[21,22] templating nanomaterials,[23−25] and gelation.[26−28] This interest stems mainly from their spontaneous formation and long-term stability, when compared to most lipidic vesicle formulations.[29]

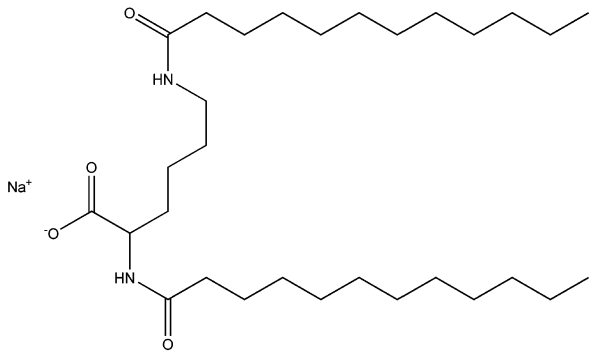

Figure 1. Chemical structure of sodium N^{α},N^{ϵ}-didodecanoyl-L-lysinate, designated here as 12-Lys-12.

The study of the micelle-to-vesicle transition is also of particular relevance for biological systems where often the extraction of proteins from cell membranes is required. In this step, some denaturation of the proteins may occur or they may become unstable if exposed to the hydrophilic solvent. Since removal of the micellizing surfactant poses some difficulties (and in some cases is even undesirable), the assembly of the proteins in a hydrophobic moiety[30] or its selective positioning in an amphiphilic domain (partially hindered and partially exposed to the solvent) may allow it to keep its native conformation or even its renaturation,[31] while simultaneously mimicking biomembrane conditions.

Bilayer solubilization usually involves the addition of a micellizing surfactant[32] to the previously assembled system. It starts with the partition of the detergent between the bilayer and the bulk, and ultimately with the disruption of the bilayers, and formation of mixed micelles. This apparently simple process can take place via two paths. One is direct, involving the formation of micelles from vesicles, while the other involves phase separation, with the vesicular and micellar regions split

* Address correspondence to this author. E-mail: efmarque@fc.up.pt. Phone: +351 226082835. Fax: +351 226082959.
[†] University of Porto.
[‡] Lund University.

10.1021/jp061946j CCC: $33.50
Published on Web 08/24/2006

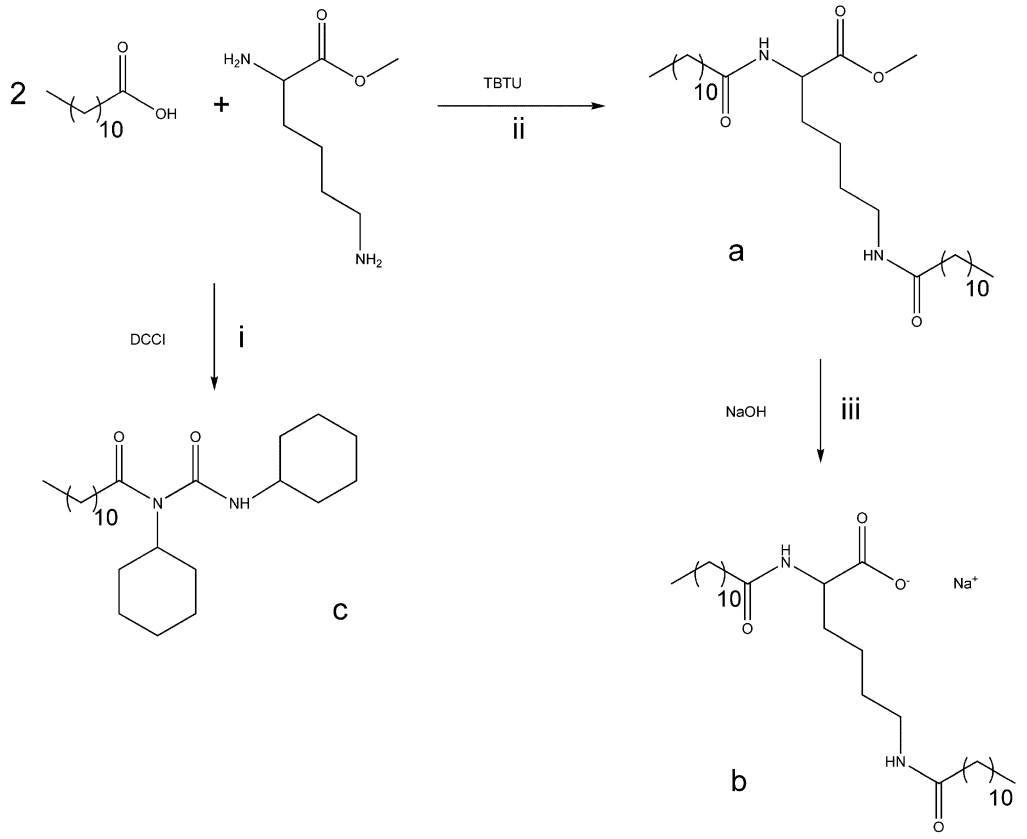

Figure 2. Synthetic path for the 12-Lys-12 surfactant (see text for a, b, and c).

by a two-phase region.[13,33,34] The latter usually occurs when there is significant growth of the mixed micelles.[34]

In this work, the ability of the novel 12-Lys-12 surfactant to form, in aqueous solution, catanionic vesicles with an oppositely charged synthetic surfactant, has been thoroughly investigated. As will be described, vesicles indeed form spontaneously in the cationic-rich side for a narrow region of compositions, limited by a precipitation region and a micellar phase. The morphology of the aggregates formed as the surfactant mixing ratio is varied, and in particular the micelle-to-vesicle transition, has also been probed by NMR and imaging techniques.

2. Material and Methods

2.1. Synthesis. The lysine-derived surfactant was synthesized according to the following reaction scheme:

Compounds **a** (N^{α},N^{ϵ}-didodecanoyl-L-lysine methyl ester) and **b** (N^{α},N^{ϵ}-didodecanoyl-L-lysine sodium salt) were synthesized by standard peptide chemistry methods (Figure 2). Dicyclohexylcarbodiimide (DCCI)-mediated condensation[35] of L-lysine methyl ester with lauric acid (scheme i) did not lead to the desired product (**a**), as formation of *N*-acylurea (**c**) was the favored process (data not shown). This problem was solved by the use of 2-(1*H*-benzotriazole-1-yl)-1,1,3,3-tetramethyl uronium tetrafluoroborate (TBTU)[36] as condensation agent, which allowed us to obtain **a** in high yields (scheme ii). Compound **b** was readily obtained by saponification of **a** with sodium hydroxide at room temperature (scheme iii), as described by Bodanszky et al.[37]

2.2. Sample Preparation. DTAB from Acros Organics (99% purity) was used. Samples made exclusively for the mapping of the phase behavior were prepared by mixing the appropriate amount of individual surfactant solutions and carefully homogenizing afterward. For the preparation of samples for NMR scanning, separate solutions of DTAB and 12-Lys-12, both at 0.5 wt %, in deuterated water (Armar Chemicals), were used (with 3% of high purity Millipore water for better monitoring the echo decay of water). After mixing, the samples were homogenized and left at rest for 2 days prior to the NMR scans. The total surfactant concentration was kept constant (and equal to 0.5 wt %), whereas the composition of the mixture was varied by varying the molar fraction of DTAB, defined as $X_{DTAB} = n_{DTAB}/(n_{DTAB} + n_{12-Lys-12})$.

2.3. Polarized Light Microscopy (PLM). PLM observation of samples was done at room temperature with an Olympus BX51 polarized light microscope equipped with a Differential Interference Contrast (DIC) system.

2.4. Differential Scanning Calorimetry (DSC). DSC scans were made with a Setaram microDSCIII high-sensitivity calorimeter. Two steel batch cells were used, one containing the 12-Lys-12 and the other neat water as reference.[38,39] The scan rate was of 0.5 K min^{-1} and the reported results refer to heating scans.

2.5. NMR. ^{1}H NMR and diffusion measurements were recorded at 25 °C with a 200 MHz Bruker DMX200 spectrometer, equipped with a diffusion probe with maximum field gradient of 9 T m^{-1}. The typical pulsed field gradient (PFG) NMR sequence for measuring self-diffusion coefficients is based on the Hahn spin−echo and is known as the Stejskal−Tanner experiment, as described in detail elsewhere.[40,41] The Hahn echo sequence was used for the measurement of the water self-diffusion coefficient in the solution samples, while the stimulated echo sequence was used for the surfactant.[40,41]

2.6. Cryo-TEM. Cryo-TEM imaging was used to visualize the aggregates present in the solution samples with different mixing ratios. In this technique a copper grid with a thin film of the sample was quickly vitrified by immersion in liquid

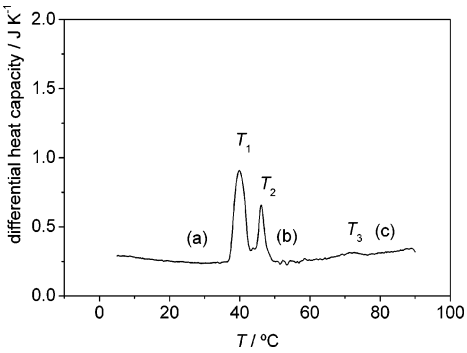

Figure 3. DSC scan of a 0.5 wt % sample of 12-Lys-12 in water (scan rate 0.5 K min^{-1}). For the significance of regions a−c and temperatures T_1−T_3, see text.

ethane.[42,43] The sample was then carefully transferred to a Philips CM 120 Bio-Twin transmission electron microscope under liquid nitrogen environment.

3. Results and Discussion

3.1. Aggregation Behavior of 12-Lys-12 in Water. A preliminary study of dilute dispersions of 12-Lys-12 in water has been carried out, prior to the investigation of the catanionic 12-Lys-12/DTAB mixture. Despite its relatively short alkyl chain length, the surfactant is insoluble at room temperature and is neither a micellizing nor a bilayer-forming (swelling) amphiphile. It solubilizes at high temperature (around 40−45 °C, depending on concentration) to yield bluish translucent solutions. Undercooled solutions at room temperature show the presence of large supramolecular self-assemblies, as shown below.

A DSC study is presented for a 0.5 wt % surfactant sample (Figure 3). PLM imaging was carried out in parallel to clarify the series of peaks observed in the DSC thermogram.

At 25.0 °C, Figure 3, region a, only dispersed crystals are visible. At 39.9 (T_1) and 46.1 °C (T_2) two sharp transitions are seen, and with increasing temperature, at 71.3 °C (T_3), another transition is observed. According to the PLM observations, the first transition, T_1, coincides with the onset of the "melting" of the dispersed crystals. Above this temperature, when the solution is allowed to equilibrate at 42.0 °C, tubules start to assemble and simultaneously there is a gradual disappearance of the crystals. Above T_2, no visible changes occur and only tubules are visible (Figure 3, region b). These observations suggest that the peaks are associated with the complete melting transition of the surfactant hydrocarbon chains, which may comprise an intermediate gel state between T_1 and T_2. The total enthalpy value for the two peaks is ca. 44 kJ mol^{-1}, giving roughly 2 kJ per mole of CH_2 (excluding the carbon spacer), a value that is typical for the melting of surfactant alkyl chains.[38,44] Only above the T_3 temperature value (71.3 °C) are the tubules seen in the microscope to gradually disappear. In the thermogram, a slight lump from the baseline is seen for the 68−76 °C range.

Upon cooling, pronounced hysteresis is observed, with the solution remaining bluish between 30 min and 1 h at room temperature, after which it turns white and very viscous. An undercooled solution of tubules is seen in Figure 4. The cross section diameter of these structures is about 0.9−1.3 μm with a very long length. The high viscosity of the sample is due to the high degree of entanglement of the tubules.

These supramolecular structures seem to be common to a number of surfactants with large headgroups that can form intermolecular hydrogen bonding.[6−9,45] Here, molecular packing

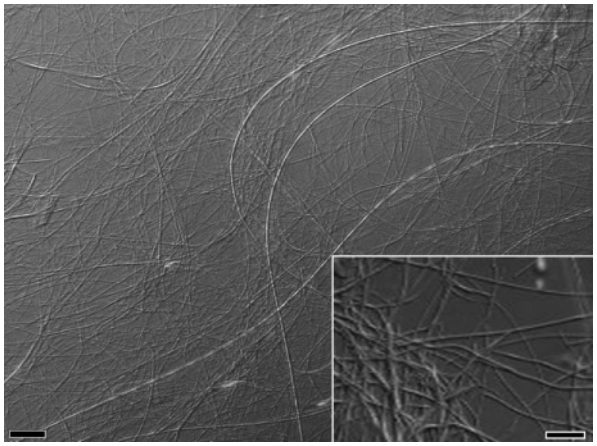

Figure 4. Polarized light microscopy imaging of a 0.5 wt % sample of 12-Lys-12 in water, at room temperature. Scale bars: left 20 μm, right 10 μm.

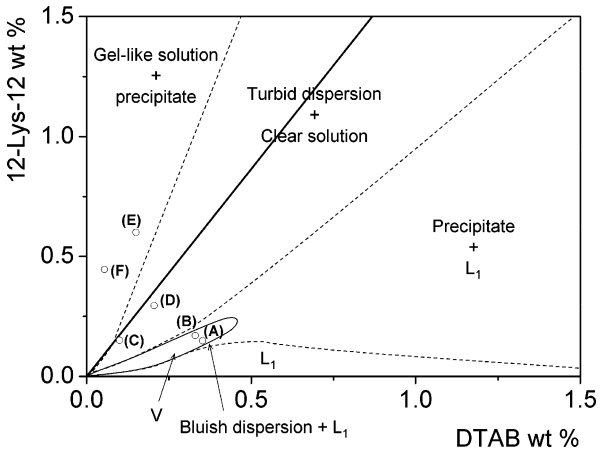

Figure 5. Phase behavior for the catanionic system 12-Lys-12/DTAB/water at 25 °C, where L_1 denotes a colorless solution phase (micelles) and V a bluish solution phase, containing vesicle aggregates. Imaging of the compositions designated by (A)−(F) is shown in Figure 6.

parameters play an important role, and depending on the headgroup nature and on hydrocarbon chain length, the aggregates may vary from tubes to helixes, with conformations such as strands and ribbons also being frequently found.[6−9]

By comparison to similar systems, the stability of the tubular structures found for 12-Lys-12 seems to be associated both with the double-chained nature of the surfactant and the hydrogen bonding between headgroups. The tubules are first fairly rigid self-assemblies with a high degree of molecular order, with tightly packed solid-like chains. The individual surfactant molecules probably assemble helicoidally and, in view of their section area, the tubules are hollow. They seem to remain intact upon chain melting, and only when the temperature is high enough for significant disruption of intra-aggregate hydrogen bonding do they disassemble to yield smaller aggregates. Further studies to clarify the molecular structure of the tubules are in progress and will be reported elsewhere.

3.2. Catanionic 12-Lys-12/DTAB Mixture: Phase Behavior. The phase behavior for the system 12-Lys-12/DTAB/water is depicted in Figure 5, where the straight line represents equimolar (and equicharged) compositions, dividing the diagram into cationic-rich and anionic-rich areas. Two single-phase regions are observed in the cationic-rich side: a region of colorless low viscous solutions and a narrow lobe containing bluish translucent solutions. In addition, there are four heterogeneous regions, which will be described in detail below.

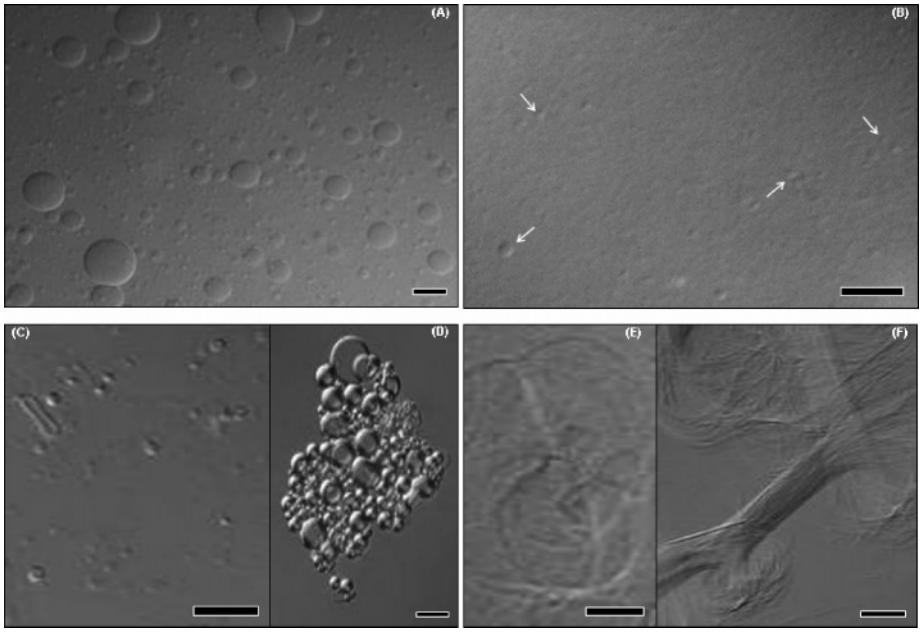

Figure 6. Light microscopy imaging of samples indicated in Figure 5. Scale bars: (A, B) 20 μm; (C−F) 10 μm. Composition of the samples in wt % 12-Lys-12/wt % DTAB: (A) 0.15/0.35; (B) 0.17/0.33; (C) 0.15/0.10; (D) 0.30/0.20; (E) 0.60/0.15, and (F) 0.45/0.05.

On the DTAB-rich side, the micellar region L_1 comprises colorless solutions of low viscosity, implicating that the micellar growth upon gemini incorporation is not significant. Increasing concentration of the anionic compound leads to the formation of a small amount of precipitate that sediments at the bottom of the sample vials (region precipitate + L_1). This precipitate appears to be of an amorphous nature when visualized by PLM, without any visible sign of structural anisotropy.

Up to a total surfactant concentration of 0.5 wt %, between the micellar region and the bluish lobe, a two-phase region can be observed. The phase separation occurs in the range $X_{DTAB} = 0.81-0.83$ and is a slow process, becoming visible one week after sample preparation. The samples in this region show a bluish, slightly turbid, upper phase, with a lower clear solution phase. Seen by PLM, the top phase exhibits droplets of considerable size (Figure 6A), whereas the lower phase is isotropic and no aggregates are detected in the light microscope.

For $X_{DTAB} < 0.81$, phase separation no longer occurs, and bluish solutions form. These solutions contain spontaneously formed vesicles, which remain stable for a long period of time. Figure 6B shows the aggregates present in this region of the phase map. Some large micron-sized vesicles are seen (white arrows), possibly resulting from long-term aggregation of smaller vesicles. Cryo-TEM of a sample in this region was also carried out to confirm unequivocally the presence of smaller vesicles (Figure 11, discussed further below).

Upon increasing the concentration of gemini surfactant in the system, phase separation occurs with samples forming a turbid upper phase and a clear bottom phase. Visualization of this phase shows that the top turbid portion is made of aggregated vesicles and wormlike bilayer aggregates, where an asymmetric partition of the solvent is expected[46] (Figure 6C).

Further on the gemini-rich side, a gel-like phase is seen, retaining a white cloudy precipitate in growing amount with increasing 12-Lys-12 concentration. This is a two-phase region where a bluish gel-like matrix comprised of highly entangled tubules holds clusters of white flocculate (Figure 6E,F).

3.3. DTAB-Rich Side: Microstructure Evolution. The microstruture evolution as 12-Lys-12 is added was probed in detail by ^{1}H NMR (1D spectra and self-diffusion) and cryo-TEM. The samples have a total surfactant concentration of 0.5 wt %, and range in composition from the neat DTAB micellar region toward the vesicle lobe. ^{1}H NMR spectra (Figure 7) yield preliminary qualitative information on the evolution of aggregate size. In the range $X_{DTAB} = 0.85-1.00$, sharp proton peaks are obtained, consistent with relatively small aggregates in solution (micelles), while significant peak broadening is seen for $X_{DTAB} \leq 0.81$. In the range $X_{DTAB} = 0.81-0.83$, phase separation occurs. The peak broadening is a consequence of a slowdown of the overall dynamics in the system (hence, faster T_2 relaxation) and it signals the formation of much larger aggregates in solution (vesicles).

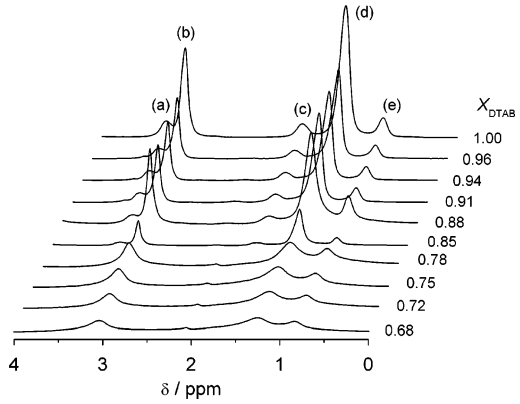

Figure 7. Comparison of the ^{1}H NMR spectra of 12-Lys-12/DTAB solutions with varying mixing ratio (0.5 wt % total surfactant). Peak assignment: (a) $^{\alpha}C\boldsymbol{H}_2N^+(CH_3)_3$; (b) $N^+(C\boldsymbol{H}_3)_3$; (c) $^{\beta}C\boldsymbol{H}_2$-$CH_2N^+(CH_3)_3$; (d) $(C\boldsymbol{H}_2)_n$; (e) $(CH_2)_nC\boldsymbol{H}_3$.

Further insight into the microstructure evolution can be obtained from the variation of the self-diffusion coefficients of both water and surfactant with composition. Figure 8 shows the reduced diffusion coefficients for water, D_r, given by the ratio D/D_o, where D and D_o are respectively the measured and the neat water diffusion coefficient, at the same temperature. For all samples, monoexponential echo decays were observed. In the case of vesicle-containing solutions this fact indicates a situation of fast exchange, within the NMR time scale, between

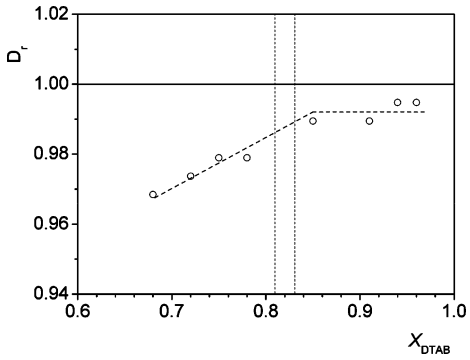

Figure 8. Reduced water diffusion coefficients, D_r, as a function of DTAB molar ratio for 12-Lys-12/DTAB solutions (0.5 wt % total surfactant). The dashed line is a guide for the eye. The vertical lines indicate the range where phase separation occurs.

water inside the vesicles and bulk water.[14,47,48] The majority of vesicles must therefore be single-walled.[48]

In the range $X_{DTAB} = 1.00-0.85$, D_r remains practically constant and close to unity, indicating the presence of (small) micelles giving rise to a low obstruction factor.[48] For $X_{DTAB} \leq 0.85$ a break in the trend occurs, with D_r decreasing gradually with gemini addition.

This decrease is consistent with the changeover in the ^{1}H-spectra and the formation of vesicles which are able to slow down the water self-diffusion. Given the low surfactant concentration, the reduction in D_r is assigned to entrapment rather than obstruction effects and is explained by an increase either in average vesicle size or in vesicle concentration at constant size. The two vertical dashed lines in Figure 8, in the range $X_{DTAB} = 0.81-0.83$, delimit the two-phase region, as previously described.

With respect to surfactant self-diffusion, monoexponential decays are obtained for peak b in the spectra of Figure 7, assigned to DTAB, whereas biexponential echo-decays occur for peaks d and e, which have a contribution from both surfactants. Typical decays corresponding to peak d, the main $(CH_2)_n$ signal, are represented in Figure 9a. As inferred from Table 1, the fast component of the biexponential decays is assigned to DTAB. In Figure 9b, it can be observed that, upon increasing concentration of 12-Lys-12, D_{DTAB} gradually decreases while for $X_{DTAB} \leq 0.85$ it remains constant, within experimental error, at $(3.3-3.5) \times 10^{-10}$ m^2 s^{-1}. Regarding the slow diffusing component, assigned to 12-Lys-12, a steeper reduction of the diffusion coefficient is observed, until a "plateau" at $(0.8-1.0) \times 10^{-11}$ m^2 s^{-1} is reached.

The first set of diffusion coefficients for both DTAB and gemini, in the range $X_{DTAB} = 0.85-1.00$, is once again consistent with micelles of relatively small size. The DTAB diffusion is faster due to the averaging effect of free monomers of DTAB (CMC = 15 mM), while the gemini, being all bound in the micelle, diffuses more slowly with the aggregate. The decrease in the diffusion of both surfactants, upon gemini addition, is a consequence of the increase in micellar size.

For the range $X_{DTAB} = 0.68-0.81$, vesicles are known to be present in solution, from the cryo-TEM imaging (Figure 11), and this is confirmed by the diffusion coefficient of gemini. Furthermore, micelles most likely also coexist with these vesicles, since D_{DTAB} values are too high for a vesicle-only solution. An averaged diffusion coefficient between free DTAB and vesicle-bound DTAB would be somewhat lower than observed due both to the low concentration of monomers (on account of the typical synergistic CMC reduction in catanionic mixtures[49]) and the slow diffusion of vesicles. Thus the observed diffusion must stem from an averaged value between small DTAB-rich micelles and mixed vesicles, as discussed further below.

3.4. Aggregate Size Determination by NMR and Cryo-TEM. Water and surfactant diffusion coefficients, complemented by cryo-TEM micrographs, can be used to assess the vesicle size distribution.

In the case of fast exchange of water, a single population-weighted average diffusion coefficient is given by[40]

$$D = p_{ves}D_{ves} + (1 - p_{ves})D_{bulk} \quad (1)$$

where D is the measured water diffusion coefficient, p_{ves} is the fraction of water inside the vesicles, D_{ves} is the diffusion coefficient of the entrapped water (equal to that of the vesicle, for small unilamellar vesicles), and D_{bulk} is the diffusion coefficient of bulk water. An estimation of the vesicle size can be made from the volume fraction of vesicles, Φ_{ves}. D_{bulk} in eq 1 can be set to AD_o, where A is an obstruction effect parameter, A, given by[50]

$$A = \frac{1}{1 + (\Phi_{ves}/2)} \quad (2)$$

where Φ_{ves} is vesicle volume fraction. Neglecting the first term of eq 1, since $p_{ves}D_{ves}$ is much smaller than D_o and equating p_{ves} with Φ_{ves}, since the vesicle radius is larger than the bilayer thickness, eq 1 can be rearranged to yield

$$\Phi_{ves} = 2\frac{1 - D_r}{2 + D_r} \quad (3)$$

where $D_r = D/D_o$. By simple geometrical calculations, one can get the vesicle radius, R_{ves}, by

$$R_{ves} = \frac{6\Phi_{ves}}{CN_A\langle A_o\rangle} \quad (4)$$

where C is the surfactant concentration, N_A is the Avogadro number, and $\langle A_o\rangle$ is the average headgroup area. For the average headgroup area, we estimated a vesicle gemini/DTAB molar ratio of 1:2 and a weighted average headgroup area based on 25 Å^2 for DTAB[34,51,52] and 75 Å^2 for 12-Lys-12. The obtained radii are given in Table 1.

For the calculation of the aggregate size based on surfactant diffusion, the 12-Lys-12 coefficients were employed since this surfactant resides only in the aggregate (micelle or vesicle). The hydrodynamic aggregate radius can be obtained from the Stokes−Einstein equation, assuming a spherical aggregate:

$$R_H = \frac{k_BT}{6\pi\eta D} \quad (5)$$

with k_B as the Boltzman constant, T as the absolute temperature, η as the solvent viscosity, and D the micelle diffusion coefficient.

From Table 1 and Figure 10 it can be seen that the mixed micelles increase gradually in size until $X_{DTAB} = 0.85$. Since the solutions are colorless and have low viscosity, it is unlikely that vesicles are present, unless they are fairly small or scarce in concentration. More likely, some form of elongated micelles are formed, since in systems where the micelle−vesicle transition occurs via phase separation (as is the case here), significant micellar growth is seen prior to the two-phase region.[34] Thus, we note that the radii calculated by using

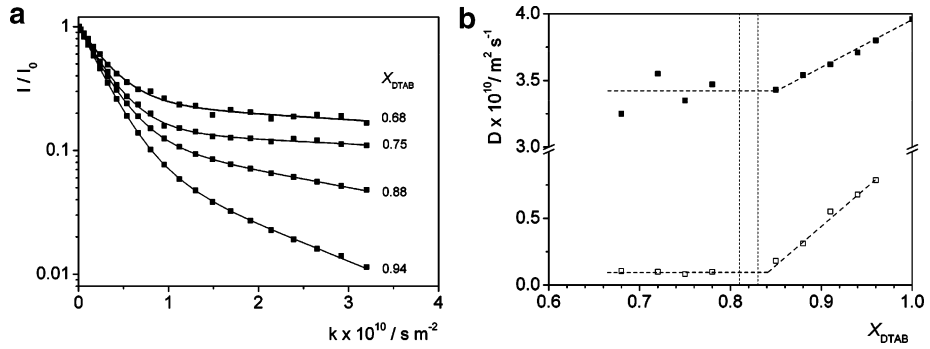

Figure 9. Surfactant self-diffusion measurements at 25 °C for 12-Lys-12/DTAB solutions (0.5 wt % total surfactant). (a) Biexponential fitting curves for the echo attenuation of the main $(CH_2)_n$ signal of selected samples, as a function of the field gradient strength (subsumed in the parameter k, defined as usual[14,40,41]). (b) Diffusion coefficients of the fast (filled squares) and slow components (empty squares) obtained from the echo decays as a function of DTAB molar fraction; the vertical lines indicate the range where phase separation occurs.

TABLE 1: Variation of D_{DTAB}, D_{fast}, and D_{slow} (from biexponential peaks) and of the Aggregate Size as a Function of DTAB Molar Fraction, at 25 ° C (0.5 wt % total surfactant)

phase region	X_{DTAB}	$10^{10}D_{DTAB}$/ $m^2\ s^{-1}$	$10^{10}D_{fast}$/ $m^2\ s^{-1}$	$10^{10}D_{slow}$/ $m^2\ s^{-1}$	R_{agg}[a]/ nm	R_{ves}[b]/ nm
L_1	1.00	3.96			2.0	
	0.96	3.80	3.85	0.79	2.5	
	0.94	3.71	3.76	0.69	2.9	
	0.91	3.62	3.69	0.55	3.5	
	0.88	3.54	3.58	0.31	6.3	
	0.85	3.43	3.52	0.18	11	
V	0.78	3.47	3.63	0.098	20	36
	0.75	3.35	3.46	0.083	24	32
	0.72	3.36	3.55	0.099	20	37
	0.68	3.25	3.30	0.11	19	40

[a] Calculated from the D_{slow} values and the Stokes−Einstein equation. [b] Calculated from water reduced diffusion coefficient for a vesicle molar composition of 12-Lys-12/DTAB 1:2.

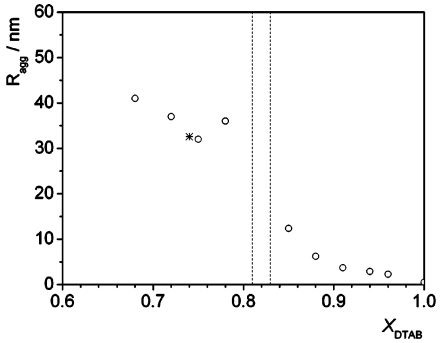

Figure 10. Aggregate size as a function of DTAB molar fraction (0.5 wt % total surfactant), with values in the L_1 and V region calculated from surfactant and water reduced self-diffusion coefficients, respectively. The asterisk denotes the vesicle average radius determined from cryo-TEM micrographs. The vertical lines indicate the range where phase separation occurs.

Stokes−Einstein are essentially qualitative due to the deviation from the spherical shape. For $X_{DTAB} < 0.81$, a significant size increase occurs, in agreement also with the ^1H peak broadening and the break in water diffusion. Moreover, the radii are entirely consistent with vesicles, being in the range of 30−40 nm. The discrepancy observed with those calculated from water diffusion (Table 1) cannot be considered unusual, just reflecting the accuracy in modeling.

Cryo-TEM imaging of this system, as illustrated in Figure 11, was also done, providing a coherent picture together with the NMR results and yielding further assessment of vesicle sizes.

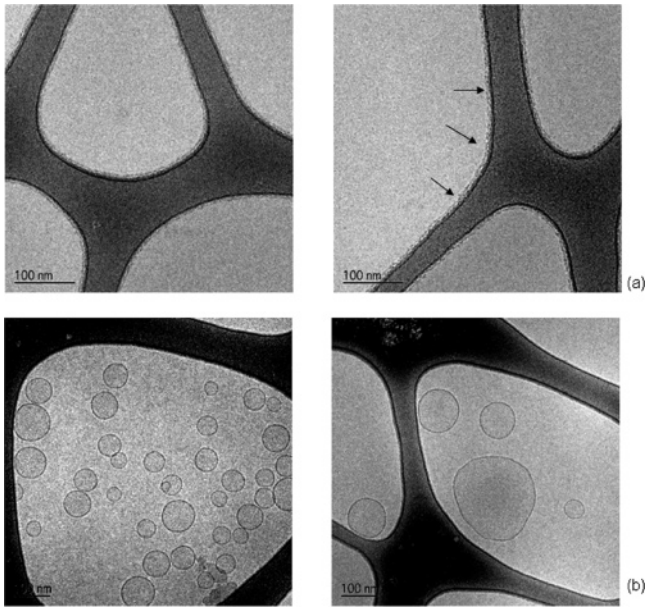

Figure 11. Cryo-TEM imaging of 12-Lys-12/DTAB solutions (0.5 wt % total surfactant) with: (a) $X_{DTAB} = 0.94$ (arrows point the micelles adsorbed to the carbon film) and (b) $X_{DTAB} = 0.74$.

At $X_{DTAB} = 0.94$, micelles are seen, mainly on the borders of the carbon film. Since the carbon film of the grids was hydrophilically modified by the glow-discharge method, acquiring a net negative charge, it was expected that the net positive micelles would adsorb on the film surface.

Imaging of the sample at $X_{DTAB} = 0.74$ shows that small, spherical, and single-walled vesicles are present in the system. They are relatively polydisperse and can be found over the entire grid, appearing not to be attracted by or adsorbed to the carbon film. The size distribution of a count of 386 vesicles is plotted in Figure 12. A log-normal distribution function of vesicle radius r could be reasonably fitted, according to

$$P(R) = \frac{1}{\sqrt{2\pi}wR}\exp[-(\ln R - \ln R_m)^2/2w^2] \qquad (6)$$

where R_m is the median vesicle radius and w is the distribution width (for a monodisperse sample $w = 0$). The mean vesicle radius is given by

$$\langle R\rangle = R_m \exp(w^2/2) \qquad (7)$$

A mean value of 33 ± 1 nm was obtained for the vesicle radius. As cryo-TEM provides images that are simple 2D

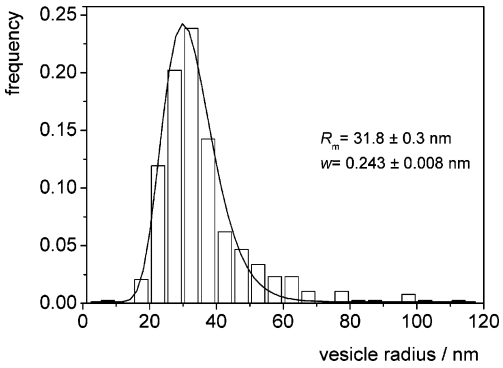

Figure 12. Size distribution for the 12-Lys-12/DTAB catanionic vesicles, obtained from cryo-TEM imaging ($X_{DTAB} = 0.74$, 0.5 wt % total surfactant). Log-normal fitting of the distribution, with the obtained R_m and w values, denoted by the solid line ($R^2 = 0.973$).

projections of the vesicles, the size obtained by the fitting is solely a number-weighted distribution, representing the most accurate value for the vesicle's radius.[53,54]

Preliminary DLS measurements of the same vesicle solution returned an apparent hydrodynamic radius of ca. 42 nm (data not shown). A slightly higher radius is expected from DLS, as the scattering is weighted by the size, and not by the number of vesicles. The two values (33 and 42 nm) can be considered to agree well with the average radius obtained from water self-diffusion (32 nm), bearing in mind the polydispersity of the system. Here we note that the latter was calculated for a constant composition of the vesicles within the vesicular region. Therefore, we argue that the catanionic vesicles have an approximate 12-Lys-12/DTAB molar ratio of 1:2, thus holding a net positive charge. Other composition ratios, such as 1:3, 1:1, or 2:1, would not be consistent with sizes obtained either by NMR or cryo-TEM (e.g., a 2:1 ratio would imply larger vesicles, slower diffusion for 12-Lys-12, and much faster diffusion for DTAB).

3.5. Vesicle Formation and Stability. Various methods based on strong energy input (mechanical or chemical) are used for the preparation of phospholipid-based vesicles, which basically imply the bending of bilayers with zero mean spontaneous curvature (i.e. flat bilayers) to a nonzero value. This energy cost can be evaluated by the curvature free energy per unit of area[55] given by

$$f_c = 2k_c(c - c_0)^2 + \bar{k}_c C \qquad (8)$$

where k_c is the mean curvature constant, c is the mean curvature at a given point ($c = {}^1/_2(c_1 + c_2)$), $\bar{k}_c$ is the Gaussian curvature constant, and C is the Gaussian curvature.

The free energy cost increases with both the curvature value and bilayer stiffness, with this last parameter being mainly dependent on the surfactant structure. This type of vesicle, either small and unilamellar or giant and multilamellar (onion-like), occurs in a metastable stable, kinetically trapped in a higher energy state than the original lamellar phase.[29] With time, these are expected to fuse, eventually reforming the primitive lamellar phase, or to ripe in mechanism similar to that of Ostwald ripening.[56] While the ripening process is influenced by the monomer dynamics in solution and solubility, the fusion phenomenon is more related to the vesicle properties, namely charge and curvature/size.

Catanionic vesicles, such as the 12-Lys-12/DTAB, are spontaneously produced, in the sense that no significant energy input is required aside from gentle shaking of the samples. Furthermore, their formation and properties strongly suggest that they can exist at thermodynamic equilibrium. Within the confines of existing models for vesicle stability in catanionic systems, the stabilization is thought to stem directly either from a favorable curvature energy, giving rise to small vesicles of low polydispersity, or from translational entropy, if the bending modulus $K = 2k + \bar{k}$ is relatively low (of the order of k_BT), in which case large and polydisperse vesicles form.

Spontaneous curvature values different from zero can, for instance, be attained when asymmetry in the bilayer constitution occurs, as proposed by Safran and co-workers.[17,57] This becomes possible in catanionic systems. The uneven distribution of the two species between the inner and the outer layer can result in the reduction of the curvature energy, even for systems with relatively high stiffness, i.e., high bending modulus K favoring the spherically curved aggregates, comparatively to flat bilayers. For the catanionic systems, such nonideal mixing could result from the electrostatic interactions between oppositely charged headgroups leading to the formation of a neutral equimolar complex and favorable mixing entropy resulting from counterion release. Vesicles with a well-defined size and bilayer composition could thus constitute the most stable state of the system for a given mixing ratio.[17]

The 12-Lys-12/DTAB catanionic vesicles form in a relatively narrow mixing ratio range, with excess DTAB. In this sense, and given that DTAB solubility in water is significantly higher than that of the gemini surfactant, it is plausible to assume that the relative composition of the vesicles should not vary dramatically with varying mixing ratio, in order for the aggregates to preserve their most favorable curvature. This does not exclude a certain degree of polydispersity. This hypothesis appears to be supported by the diffusion-NMR data, which does not show a significant size variation of the vesicles.

4. Conclusions

It has been shown that the newly synthesized 12-Lys-12 surfactant forms large tubules in aqueous solution above room temperature, giving rise to very viscous solutions. Stable catanionic vesicles can be formed by mixing this amphiphile with DTAB, for an excess of the cationic surfactant. Combined phase behavior, cryo-TEM, and NMR results have shown that in the DTAB-rich side micelle-to-vesicle transition takes place via a discontinuous process, involving first limited micellar growth and then phase separation. For $0.68 \leq X_{DTAB} \leq 0.80$, unilamellar catanionic vesicles are formed and from the self-diffusion results it is inferred that they coexist with DTAB-rich micelles. The vesicles are fairly polydisperse, with an average size on the order of 30−40 nm.

Acknowledgment. E.F.M. and P.G. kindly acknowledge Fundação para a Ciência e Tecnologia (F.C.T.) for financial support through CIQ(UP) and also F.C.T./FEDER through the research project POCTI/QUI/44296/2002. R.O.B. also acknowledges F.C.T. for the grant BD SFRH/BD/16380/2004. O.S. thanks the Swedish Research Council for financial support.

Supporting Information Available: Synthesis details for **2a** and **2b**. This material is available free of charge via the Internet at http://pubs.acs.org.

References and Notes

(1) Menger, F. M.; Keiper, J. S. *Angew. Chem., Int. Ed.* **2000**, *39*, 1906.
(2) Zana, R. *Adv. Colloid Interface Sci.* **2002**, *97*, 205.
(3) Pinazo, A.; Wen, X.; Pérez, L.; Infante, M.-R.; Franses, E. I. *Langmuir* **1999**, *15*, 3134.

(4) Infante, M. R.; Perez, L.; Pinazo, A.; Clapes, P.; Moran, M. C.; Angelet, M.; Garcia, M. T.; Vinardell, M. P. *C. R. Chim.* **2004**, *7*, 592.
(5) Benavides, T.; Martínez, V.; Mitjans, M.; Infante, M. R.; Moran, C.; Clapés, P.; Clothier, R.; Vinardell, M. P. *Toxicology* **2004**, *201*, 87.
(6) Fuhrhop, J.-H.; Helfrich, W. *Chem. Rev.* **1993**, *93*, 1565.
(7) Mohanty, A.; Dey, J. *Langmuir* **2004**, *20*, 8452.
(8) Imae, T.; Takahashi, Y.; Muramatsu, H. *J. Am. Chem. Soc.* **1992**, *115*, 3414.
(9) Imae, T.; Hayashi, N.; Matsumoto, T.; Tada, T.; Furusaka, M. *J. Colloid Interface Sci.* **2000**, *225*, 285.
(10) Kaler, E. W.; Murthy, A. K.; Rodriguez, B. E.; Zasdzinski, J. A. N. *Science* **1989**, *245*, 1371.
(11) Kaler, E. W.; Herrington, K. L.; Murthy, A. K.; Zasadzinski, J. A. *J. Phys. Chem.* **1992**, *96*, 6698.
(12) Chirovulu, S.; Israelachvili, J. N.; Naranjo, E.; Xu, Z.; Zasadzinski, J. A.; Kaler, E. W.; Herrington, K. L. *Langmuir* **1995**, *11*, 4256.
(13) Yatcilla, M. T.; Herrington, K. L.; Brasher, L. L.; Kaler, E. W.; Chiruvolu, S.; Zasadzinski, J. A. *J. Phys. Chem.* **1996**, *100*, 5874.
(14) Marques, E. F.; Regev, O.; Khan, A.; Miguel, M. d. G.; Lindman, B. *J. Phys. Chem. B* **1998**, *102*, 6746.
(15) Marques, E. F.; Regev, O.; Khan, A.; Miguel, M. d. G.; Lindman, B. *J. Phys. Chem. B* **1999**, *103*, 8353.
(16) Marques, E. *Langmuir* **2000**, *16*, 4798.
(17) Safran, S. A.; Pincus, P.; Andelman, D. *Science* **1990**, *248*, 354.
(18) Yuet, P. K.; Blankschtein, D. *Langmuir* **1996**, *12*, 3802.
(19) Vautrin, C. Z., T.; Schneider, M.; Tanaka, M. *J. Phys. Chem. B* **2004**, *108*, 7986.
(20) Hao, J.; Yuan, Z.; Liu, W.; Hoffmann, H. *J. Phys. Chem. B* **2004**, *108*, 5105.
(21) Dias, R. S.; Lindman, B.; Miguel, M. G. *J. Phys. Chem. B* **2002**, *106*, 12600.
(22) Dias, R. S.; Lindman, B.; Miguel, M. G. *J. Phys. Chem. B* **2002**, *106*, 12608.
(23) Hentze, H. P.; Raghavan, S. R.; McKelvey, C. A.; Kaler, E. W. *Langmuir* **2003**, *19*, 1069.
(24) Lootens, D.; Vautrin, C.; Van Damme, H.; Zemb, T. *J. Mater. Chem.* **2003**, *13*, 2072.
(25) McKelvey, C. A.; Kaler, E. W.; Zasadzinski, J. A.; Coldren, B.; Jung, H. T. *Langmuir* **2000**, *16*, 8285.
(26) Antunes, F. E.; Marques, E. F.; Gomes, R.; Thuresson, K.; Lindman, B.; Miguel, M. G. *Langmuir* **2004**, *20*, 4647.
(27) Marques, E. F.; Regev, O.; Khan, A.; Miguel, M. G.; Lindman, B. *Macromolecules* **1999**, *32*, 6626.
(28) Lee, J.-H.; Gustin, J. P.; Chen, T. H.; Payne, G. F.; Raghavan, S. R. *Langmuir* **2005**, *21*, 26.
(29) Lasic, D. D.; Joannic, R.; Keller, B. C.; Frederik, P. M.; Auvray, L. *Adv. Colloid Interface Sci.* **2001**, *89*−*90*, 337.
(30) Fernández, C.; Wüthrich, K. *FEBS Lett.* **2003**, *555*, 144.
(31) Lu, R.-C.; Xiao, J.-X.; Cao, A.-N.; Lai, L.-H.; Zhu, B.-Y.; Zhao, G.-X. *Biochim. Biophys. Acta* **2005**, *1722*, 271.
(32) Koynova, R.; Tenchov, B. *Curr. Opin. Colloid Interface Sci.* **2001**, *6*, 277.
(33) Herrington, K. L.; Kaler, E. W.; Miller, D. D.; Zasadzinski, J. A.; Chiruvolu, S. *J. Phys. Chem.* **1993**, *97*, 13792.
(34) Söderman, O.; Herrington, K. L.; Kaler, E. W.; Miller, D. D. *Langmuir* **1997**, *13*, 5531.
(35) Sheehan, J. C.; Hess, G. P. *J. Am. Chem. Soc.* **1955**, *77*, 1067.
(36) Knorr, R.; Trzeciak, A.; Bannwarth, W.; Gillesen, D. *Tetrahedron Lett.* **1989**, *30*, 1927.
(37) Bodanszky, M.; Bodanszky, A. *The practice of peptide synthesis*; Springer-Verlag: Berlin, Germany, 1984.
(38) Blume, A.; Gabriel, P. Lipid model membranes and biomembranes. In *Handbook of Thermal Analysis and Calorimetry*; Kemp, R. B., Ed.; Elsevier: Amsterdam, The Netherlands, 1999.
(39) Wadsö, I.; Gatta, G. D.; Richardson, M. J.; Sarge, S. M.; Stolen, S. Standards Calibration and Guidelines in Microcalorimetry, IUPAC Project No. 120/18/97 (Commision I.2), 1997.
(40) Söderman, O.; Stilbs, P. *Prog. Nucl. Magn Reson. Spectrosc.* **1994**, *26*, 445.
(41) Stilbs, P. *Prog. Nucl. Magn Reson. Spectrosc.* **1987**, *19*, 1.
(42) Bellare, J. R.; Davis, H. T.; Scriven, L. E.; Talmon, Y. *Electron Microsc. Technol.* **1988**, *10*, 87.
(43) Talmon, Y. *Ber. Bunsen-Ges. Phys. Chem.* **1996**, *3*, 364.
(44) Marques, E. F.; Khan, A.; Lindman, B. *Thermochim. Acta* **2002**, *394*, 31.
(45) Suzuki, M.; Owa, S.; Kimura, M.; Kurose, A.; Shirai, H.; Hanabusa, K. *Tetrahedron Lett.* **2005**, *46*, 303.
(46) Khopade, A. J.; Shenoy, D. B.; Khopade, S. A.; Jain, N. K. *Langmuir* **2004**, *20*, 7368.
(47) Price, W. S. *Concepts Magn. Reson.* **1997**, *9*, 299.
(48) Olsson, U.; Nakamura, K.; Kunieda, H. *Langmuir* **1996**, *12*, 3045.
(49) Khan, A.; Marques, E. Catanionic Surfactants. In *Specialist Surfactants*; Robb, I., Ed.; Blackie Academic and Professional, Chapman and Hall: London, UK, 1997.
(50) Jönsson, B.; Wennerström, H.; Nilsson, P. G.; Linse, P. *Colloid Polym. Sci.* **1986**, *264*, 77.
(51) Patrick, H. N.; Warr, G. G.; Manne, S.; Aksay, I. A. *Langmuir* **1999**, *15*, 1685.
(52) Scheuing, D. R.; Weers, J. G. *Langmuir* **1990**, *6*, 665.
(53) Coldren, B.; Zanten, R. v.; Mackel, M. J.; Zasadzinski, J. A. *Langmuir* **2003**, *19*, 5632.
(54) Egelhaff, S. U.; Wehrli, E.; Müller, M.; Adrian, M.; Schurtenberger, P. *J. Microsc.* **1996**, *184*, 214.
(55) Helfrich, W. *Z. Naturforsch.* **1973**, *28*, 693.
(56) Olsson, U.; Wennerström, H. *J. Phys. Chem. B* **2002**, *106*, 5135.
(57) Safran, S. A.; Pincus, P.; Andelman, A.; Makintosh, F. C. *Phys. Rev.* **1991**, *43*, 1071.